Collisional Relaxation of Superthermal Electrons Generated by Relativistic Laser Pulses in Dense Plasma

A. J. Kemp,[1,*] Y. Sentoku,[1] V. Sotnikov,[1] and S. C. Wilks[2]
[1]Department of Physics, University of Nevada, Reno, Nevada 89557, USA
[2]Lawrence Livermore National Laboratory, Livermore, California 94551, USA
(Received 31 July 2006; published 4 December 2006)

Energy relaxation of the hot electron population generated by relativistic laser pulses in overdense plasma is analyzed for densities ranging from below to 1000 times solid density. It is predicted that longitudinal beam-plasma instabilities, which dominate energy transfer between hot electrons and plasma at lower densities, are suppressed by collisions beyond solid density. The respective roles of collisional energy transfer modes, i.e., direct collisions, diffusion, and resistive return current heating, are identified with respect to plasma density. The transition between the kinetic and the collisional regimes and scalings of collisional process are demonstrated by a fully integrated one-dimensional collisional particle simulation.

DOI: 10.1103/PhysRevLett.97.235001 PACS numbers: 52.38.Ph, 52.35.Qz, 52.40.Mj, 52.65.−y

The interaction of ultrashort laser pulses of relativistic intensities $I\lambda^2 > 10^{18}$ W/cm^2 μm^2 with matter generates energetic electrons that penetrate deeply into solid targets and deposit energy on subpicosecond time scales. Understanding the transport and transfer of energy between these ''hot'' electrons and the target is important for many potential applications, as, for example, isochoric heating of solid targets to high temperatures or the fast ignition of compressed fusion targets [1,2]. The processes responsible for the energy transfer, in particular, in a recent fast-ignition experiment [3], are currently under debate. Explanations differ between anomalous kinetic- [4] and collisional effects [5].

This Letter deals with the partition of energy between hot and thermal electrons in plasma at densities ranging from just above to several thousand times critical density—defined by the location where a nonrelativistic laser pulse is absorbed in a plasma. While kinetic effects in ultrashort intense laser-matter interaction and electron beam transport through plasma have been the subject of research for many years [6], not much is known about densities beyond solid, for the following reason. The most widely used numerical model for laser-matter interaction is the particle-in-cell (PIC) model, in which the Maxwell-Vlasov kinetic equations are integrated with a finite-element method [7]. PIC simulations for plasma at greater-than-solid densities are numerically challenging because (1) the Debye length $\lambda_D = v_t/\omega_p$, which needs to be resolved in order to avoid numerical self-heating, is <1 nm for 50 eV solid-density plasma. In typical PIC simulations one initializes the plasma with keV temperatures to avoid this effect; (2) the plasma skin length $l_s = c/\omega_p$ needs to be resolved to include collective phenomena like those discussed below. In many current hybrid codes l_s is not resolved. In addition, the Coulomb collision frequency is close to the plasma frequency, so that collisional effects like resistivity or diffusion cannot be neglected.

In the following, we compare several mechanisms of energy transfer between hot and cold electrons at plasma densities beyond the critical density where the laser pulse is absorbed. We focus on a one-dimensional scenario with an appropriately resolved simulation of an electron beam traveling up a plasma density gradient that includes the effects of Coulomb collisions self-consistently [8]. We find that (i) kinetic energy transfer from an electron beam to a dense plasma is important at near-critical density, but it is suppressed by collisions at solid density and beyond; (ii) at solid density, resistive heating followed by diffusion and direct collisions between hot electrons and the background play the most important roles for energy transport and transfer; (iii) at much higher densities, diffusion and direct collisions dominate over resistive heating. We demonstrate these effects in a fully collisional, one-dimensional PIC simulation of an intense laser pulse interacting with a plasma density gradient between under-critical to 10 000 critical densities. Note that our studies are restricted to longitudinal effects. Preliminary results indicate that our conclusions apply to transverse kinetic instabilities, as observed in 2D collisional PIC simulations [9]. However, there is an ongoing discussion about the role of transverse electromagnetic modes with respect to energy transfer between an electron beam and a plasma [10].

In a first step we consider the role of longitudinal kinetic effects on the transfer of energy between a beam of particles and a background plasma. The excitation of longitudinal modes in a plasma via electric fields represents a transfer of energy from the laser-generated hot beam into the background [11]. The ''weak-beam-plasma'' instability growth rate

$$\Gamma_L \simeq 0.5\omega_p(n_b/n_p)(v_b/v_{b,\mathrm{th}})^2, \quad (1)$$

is related to the background plasma frequency $\omega_p = \sqrt{4\pi e^2 n_e/m_e}$, to $v_b/v_{b,t} \approx 1$, and the beam-to-plasma density ratio n_b/n_p [12]. For a hot beam, the thermal

velocity spread $v_{b,\mathrm{th}} > \gamma/k_r$, where γ is the cold beam growth rate. In the presence of collisions within the background plasma, however, plasma wave growth will be reduced and even suppressed as soon as the growth rate Γ_L is exceeded by the damping rate, which is defined by the electron collision frequency $\nu_e = (8\pi/3\sqrt{3m_e})(n_c e^4 \ln\Lambda)/(kT)^{3/2}$ [13]. For laser-matter interaction this will be the case near solid density. Figure 1 gives an overview over regimes of energy transfer between an electron beam at a constant density $n_b = 10^{21}$ cm^{-3} and a background plasma [14]. All rates shown assume a uniform electron beam injected into a plasma with a current density $n_c c$ in a one-dimensional geometry. Figure 1 allows two conclusions: (1) at low density the growth times for kinetic energy transfer are of the order fs, while beyond solid density the growth times are of the order of several tens of fs even without collisions; (2) collisions within the background plasma will suppress longitudinal beam-plasma instabilities at roughly solid density for all reasonable values of the background temperature. The location of the boundary between the kinetic and the collisional regimes depends on the hot electron beam density n_b and the background temperature. In our simulation below we find $n_b \approx 0.3 n_c$ in 1D. This shifts the indicated boundary to lower densities.

We now analyze the respective roles of collisional effects on energy transfer between hot and cold electrons at and beyond solid density, where kinetic effects are suppressed. We start from the Vlasov equation with a Fokker-Planck collision term for a two-temperature electron distribution in one dimension, neglecting magnetic fields and ion motion for the moment [15]; note that stopping of energetic ions can have a important effect, see below. The leading terms for the evolution of the cold temperature are: diffusion, resistive heating by the cold return current (equal in magnitude but opposite to the hot beam current), and collisions between hot and plasma electrons (drag heating)

$$\frac{3}{2} n_c \frac{\partial T_c}{\partial t} = \frac{\partial}{\partial x}\left(\kappa(T_c)\frac{\partial T_c}{\partial x}\right) + \frac{j_h^2}{\sigma(T_c)} + \frac{3}{2}\frac{n_h T_h}{\tau_e}, \qquad (2)$$

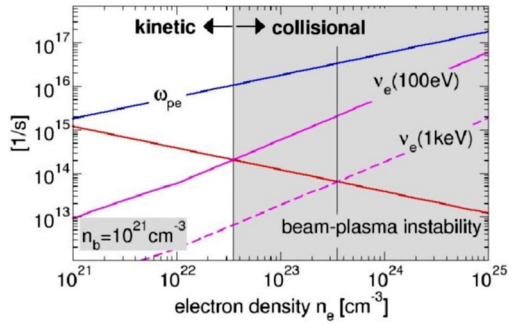

FIG. 1 (color online). Regimes of energy transfer between an electron beam with $n_b = 10^{21}$ cm^{-3} and a plasma. Plotted are the growth rate Γ_L of the hot beam-plasma instability, the cold electron-ion collision frequency ν_{ei} for 100 and 1000 eV, electron plasma frequency ω_{pe}. Kinetic modes are suppressed if $\Gamma < \nu_{ei}$, as indicated by the shaded area.

where $j_h = e n_h c$ is the hot electron current with $n_h = \alpha n_0$ and the critical density $n_0 = 10^{21}$ cm^{-3}, while $\kappa = (16\sqrt{2}/\pi^{3/2}) \times (kT)^{5/2}/(e^4 m_e^{1/2} \ln\Lambda)$ is the electron thermal conductivity, $\sigma = n_c e^2 \tau_c / m_e$ is the electric conductivity, and $\tau_e = (\nu_e)^{-1}$ is the collision time for cold electrons in a fully ionized plasma [16]. Replacing the spatial derivative with a length scale L_T of the cold temperature profile, we arrive at scalings that compare the roles of each partial contribution

$$\begin{aligned} T_{\mathrm{eV}}^{\mathrm{dr/dif}} &> 120 T_h^{-1/7} \alpha^{2/7} L_T^{4/7} n_{c,23}^{2/7}, \\ T_{\mathrm{eV}}^{\mathrm{res/dif}} &> 600 \alpha^{2/5} L_T^{2/5}, \\ T_{\mathrm{eV}}^{\mathrm{res/dr}} &> 22500 T_h^{1/3} \alpha^{2/3} n_{c,23}^{-2/3}. \end{aligned} \qquad (3)$$

Here $n_{c,23}$ stands for the cold electron density in units of 10^{23} cm^{-3}, $T_{c,\mathrm{eV}}$ for the cold electron temperature in eV and L_T is the scale length in μm. The first equation compares drag heating with diffusion, the second compares resistive heating with diffusion, and the third compares resistive with drag heating.

Figure 2 illustrates Eq. (2), assuming an electron beam at temperature $T_h = 0.4$ MeV and density $n_h = 0.3 n_0$ in a plasma with a diffusion scale length of $L_T = 10$ μm, corresponding to the simulation parameters below. The colored lines representing Eqs. (3) indicate where the leading term changes. At solid density and temperatures below several hundred eV, resistivity and diffusion dominate; drag heating only plays a role for negligible temperature gradients, i.e., at late times and deep in the target. On the other hand, at high densities $n > 10^{25}$ cm^{-3}, drag transfer dominates over resistive heating at lower temperatures. The shaded area on the top left indicates a region in phase space where the cold electron mean-free path tends to become smaller than the temperature gradient length; in this case the diffusion approximation cannot be made. The topology of Fig. 2 is independent of the free parameters (α, T_h, L_T), meaning that all three curves defined in Eqs. (3) intersect roughly in one point. Note that in the relevant density range the drift velocity of the cold return current

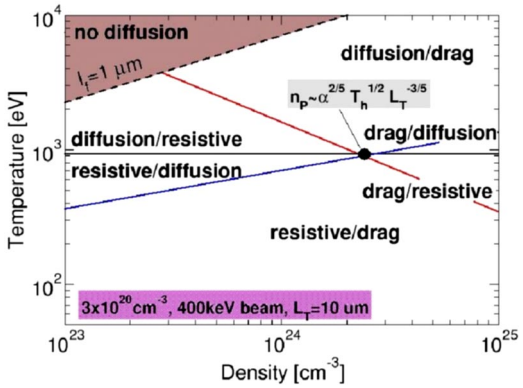

FIG. 2 (color online). Energy transfer mechanisms in the (n, T) phase plane, plotting the leading terms of Eq. (2). Diffusion is suppressed when $l_f < L_T$, indicated by the shaded area.

electrons never exceeds their thermal velocity, so that the anomalous collision frequency associated with ion acoustic turbulence excited by the return current is smaller than the ion plasma frequency and thereby much smaller than the Coulomb collision frequency. This means that collisional processes dominate over turbulence even at low-range densities [17].

These scalings are demonstrated by a fully integrated collisional one-dimensional particle-in-cell simulation with the code PICLS1D [8]. The simulations models laser produced hot electron transport in a plasma density gradient ranging from 10^{22} to $\sim 10^{25}$ cm^{-3}, as shown in Fig. 4(a) with a solid line. The 5 μm region at a density 5×10^{23} cm^{-3} at $x = 15$ μm is meant to block off the laser radiation, but it also provides hot electrons by the $\mathbf{J} \times \mathbf{B}$ acceleration, and fast ions by the sweeping acceleration mechanism [18]. Behind the slab plasma, density increases exponentially from 10^{22} to $\sim 10^{25}$ cm^{-3} over 30 μm. The plasma consists of an initially neutral mixture of electrons and protons with $m_p = 1836 m_e$. Its density at the rear of the slab plasma is sufficient to suppress the strong sheath field usually generated by hot electrons; hence there is no strong ion acceleration. The initial electron temperature is set to 160 eV, which is sufficient for an ideal Spitzer collision model for the whole range of the initial plasma density avoiding degeneracy. The driving laser pulse has a Gaussian profile with a full width half maximum pulse of $\sim$500 fs and a peak intensity 10^{19} W/cm^2. We use 500 particles per cell and weight particles to generate the density profile. At the boundaries, fields are absorbed and particles are reinjected with the initial temperature. While our mesh size of 5×10^{-3} μm is larger than the initial plasma Debye length, numerical heating is suppressed by using a third-order-interpolation scheme for both currents and fields.

Figure 3(a) shows the electron longitudinal momentum versus plasma density at their initial position, excluding hot electrons from the laser-plasma interaction. It is clearly seen that the electron momentum spreads and has a high-energy tail at densities below 10^{23} cm^{-3}, due to the longitudinal plasma wave mixing as confirmed in Fig. (4a′). The dense plasma (above 10^{23} cm^{-3}) is also heated up, but there is no high-energy tail. An otherwise identical kinetic simulation (i.e., without collisions) shows the high-energy tail even in the extremely dense plasma $>5 \times 10^{23}$ cm^{-3}, see Fig. 3(b). These results agree with our analysis in Fig. 1 showing that kinetic effects are negligible in the extreme dense plasma when Coulomb collisions are included. The boundary of the kinetic regime and collisional regime is at $\approx 10^{23}$ cm^{-3}. Figure 4(a) shows the longitudinal electron phase space at 165 fs, illustrating the excitation of the longitudinal plasma wave, as shown in Fig. (4a′). The beam density was constant with $\sim 0.3 n_c$ during laser irradiation and its temperature is about 400 keV. At densities of a few 10^{22} cm^{-3}, strong plasma waves are excited and hot electrons are mixing with the coronal plasma while losing energy. Their longitudinal momentum spreads widely and has high-energy tails.

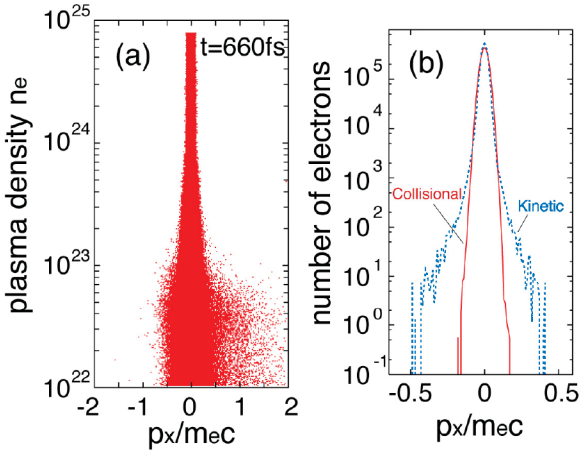

FIG. 3 (color). (a) Longitudinal electron momentum vs plasma density at the initial particle's location, i.e., local particle weight, at 660 fs. Plasma is strongly heated only up to a density of 10^{23} cm^{-3}, consistent with our analysis in Fig. 1. (b) Comparison of the longitudinal momentum at 660 fs in extremely dense plasma ($>5 \times 10^{23}$ cm^{-3}) between kinetic and collisional cases.

Figure 4(b) illustrates heating in the extremely dense area above 5×10^{23} cm^{-3}, where collisional processes dominate. Resistive heating can be observed shortly between $t = 200$–300 fs. When this mechanism is saturated, the local electron temperatures are 0.8 ($x = 36$ μm, $n_e = 5 \times 10^{23}$ cm^{-3}), 0.6 (at $x = 40$, $n_e = 10^{24}$), and 0.5 keV (at $x = 50$, $n_e = 8 \times 10^{25}$), respectively. Note that these temperatures are consistent with the threshold temperature of the region where the resistive heating is dominant in Fig. 2. Afterwards diffusion dominates the heating below 10^{24} cm^{-3} ($x < 40$ μm). This is seen in Fig. 4(b) from 400 fs to 1 ps. In the extremely dense area

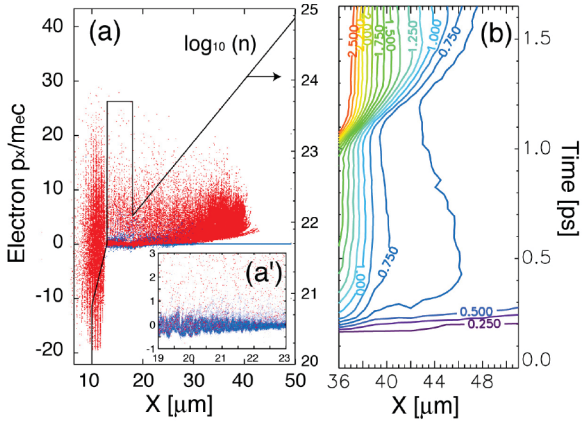

FIG. 4 (color). (a) An electron phase plot ($x - p_x$) at 165 fs. The red particles are hot electrons directly heated by the laser pulse and the blue ones are particles in coronal plasmas. (a') Closeup snap in a range of $x = 19$–23 μm. (b) A contour plot of temperature [keV] in dense plasmas, 5×10^{23} cm^{-3} (hot electrons are excluded in this plot).

($n_e = 8 \times 10^{24}\,\mathrm{cm}^{-3}$, $x > 40\ \mu$m), the electron temperature is sustained, which means the electron thermal energy is maintained by the hot electrons' drag heating, compensating for thermal energy exchange with the ions. Heating after 1 ps is due to bunches of fast ions. In addition, our kinetic results allow the conclusion that the contribution of (essentially kinetic) runaway electrons to transport is negligible, supporting the hydrodynamic approach pursued in Eq. (2). Preliminary 2D simulations give similar results to the ones shown, indicating that our conclusions for longitudinal modes also hold for those oblique with respect to the beam where the treatment is more complex than outlined above [17].

Applying our results to the experiment, we find that: (i) diffusive heat transport is a surface effect that can be neglected compared to resistive effects because the long mean-free path of the laser-generated MeV electrons (typically several 100 μm) leads to uniform heating; (ii) resistive heating can be estimated from Eq. (2), bearing in mind that the cold return current is replaced by a hot, i.e., less collisional current as soon as the fast electrons reach the rear surface. For a background density $n_e = 10^{23}\,\mathrm{cm}^{-3}$ and a current density $j_c \approx 0.1 e n_c c$ one finds $T_c(t) \approx 2 \times 10^7 t_s^{2/5}$. After roughly 30 fs this gives $T_c \approx 80$ eV, which is consistent with time-resolved spectroscopic measurements [19]; (iii) over several picoseconds, drag heating and diffusion play a significant role for the hot electron relaxation.

The resulting general picture of the energy partition between a laser-generated hot electron beam and a cold dense plasma is the following. When a laser-generated beam of hot electrons enters the solid and ionizes the material, it causes a space-charge electric field to which the plasma reacts with a return current almost immediately, i.e., on the time scale ω_p^{-1}. This current $j_h \approx (0.1\text{–}0.3) e n_0 c$ will thermalize after a time ν_{ei}^{-1} and generate a resistive electric field $E = j_h/\sigma$, where σ is the cold plasma conductivity. In the case of a thin target, resistive heating ceases after the hot electrons reach the rear surface and form a hot return current. In a thick target resistive heating dominates beam transport, raising the background temperature until diffusion sets in [20]. Diffusion balances local gradients in the background temperature in competition with resistive heating. Direct collisions between beam and plasma electrons contribute to the energy balance only after picoseconds, i.e., long after the laser pulse, or at very high density. Our assumption of a one-dimensional beam is an oversimplification that can be corrected for by using an effective hot electron density. From recent experiments [21] and kinetic two-dimensional simulations [9], we know that an electron beam will diverge in the solid at an angle of roughly 30°, causing a substantial drop in beam density and a subsequent delay in energy transfer deeper in targets. Recirculation can compensate for that only to some degree in that refluxing hot electrons overlap with later parts of the beam, enhancing their effective density in the target [22].

We conclude that the transfer of energy from laser-generated hot into thermal electrons in dense plasma is collisional, while kinetic modes of energy transfer are strongly suppressed. Resistive heating is the quickest mechanism and plays a dominant role, before either recirculation sets in or the target heats up locally so that drag heating or diffusion dominate, depending on the density and temperature gradient length scale. The former has likely been observed in Ref. [5]. Direct collisions between hot and cold electrons are important for experiments with thin foil targets ($<100\ \mu$m) over picosecond time scales including adiabatic expansion. This guides a path towards an integrated model of electron transport in large-scale dense plasma: it might be justified to underresolve the Debye length and skin length at high densities where collisional effects suppress longitudinal modes of the plasma.

A. K. and S. W. are grateful for stimulating discussions with T. Cowan (UNR), R. Freeman (OSU), R. Shepherd and M. Tabak (LLNL). This work was supported by DOE/NNSA under UNR Grant No. DE-FC52-01NV14050.

*Present address: Lawrence Livermore National Laboratory, Livermore, CA, 94551, USA.

[1] A. Saemann *et al.*, Phys. Rev. Lett. **82**, 4843 (1999).
[2] M. Tabak *et al.*, Phys. Plasmas **1**, 1626 (1994).
[3] R. Kodama *et al.*, Nature (London) **418**, 933 (2002).
[4] R. Campbell *et al.*, Phys. Rev. Lett. **94**, 055001 (2005).
[5] R. Mason, Phys. Rev. Lett. **96**, 035001 (2006).
[6] A. Pukhov and J. Meyer-ter-Vehn, Phys. Rev. Lett. **76**, 3975 (1996); M. Honda, J. Meyer-ter-Vehn, and A. Pukhov, Phys. Rev. Lett. **85**, 2128 (2000); Y. Sentoku *et al.*, Phys. Rev. Lett. **90**, 155001 (2003).
[7] C. Birdsall and A. Langdon, *Plasma Physics via Computer Simulation* (Adam Hilger, New York, 1991).
[8] Y. Sentoku *et al.*, J. Phys. Soc. Jpn. **67**, 4084 (1998).
[9] Y. Sentoku *et al.*, Phys. Rev. Lett. (to be published).
[10] A. Bret and C. Deutsch, Phys. Plasmas **12**, 082704 (2005).
[11] V. Malkin and N. Fisch, Phys. Rev. Lett. **89**, 125004 (2002).
[12] A. B. Mikhailovskii, *Theory of Plasma Instabilities* (Consultants Bureau, New York, 1974).
[13] V. Ginzburg, *The Propagation of Electromagnetic Waves in Plasmas* (Pergamon, Oxford, 1970).
[14] Note that at $n_e \gg 10^{24}\ \mathrm{cm}^{-3}$ the plasma becomes nonideal so that the simple expressions used here may be invalid.
[15] M. Glinsky, Phys. Plasmas **2**, 2796 (1995).
[16] D. Book, *NRL Plasma Formulary* (NRL, Washington, D.C., 1990).
[17] A. A. Vedenov and D. D. Ryutov, in *Reviews of Plasma Physics*, edited by M. A. Leontovich (Consultants Bureau, N.Y., 1970), Vol. 5.
[18] Y. Sentoku, T. Cowan, A. Kemp, and H. Ruhl, Phys. Plasmas **10**, 2009 (2003).
[19] S. Hansen *et al.*, Phys. Rev. E **72**, 036408 (2005).
[20] C. Deutsch *et al.*, Phys. Rev. Lett. **77**, 2483 (1996).
[21] R. Stephens *et al.*, Phys. Rev. E **69**, 066414 (2004).
[22] A. Mackinnon *et al.*, Phys. Rev. Lett. **88**, 215006 (2002).